



An intercomparison of satellite, airborne, and ground-level observations with WRF-CAMx simulations of NO₂ columns over Houston, TX during the September 2021 TRACER-AQ campaign

5 M. Omar Nawaz¹, Jeremiah Johnson², Greg Yarwood², Benjamin de Foy³, Laura Judd⁴, and Daniel L. Goldberg¹

¹Department of Environmental and Occupational Health, George Washington University, Washington, DC, 20052, USA

²Ramboll, Novato, California, 94945, USA

10 ³Saint Louis University, St. Louis, Missouri, 63103, USA

⁴NASA Langley, Hampton, Virginia, 23666, USA

Correspondence to M. Omar Nawaz (nawaz.muhammad@email.gwu.edu)

Abstract. Nitrogen dioxide (NO₂) is a precursor of ozone (O₃) and fine particulate matter (PM_{2.5}) – two pollutants that are above regulatory guidelines in many cities. Bringing urban areas into compliance of these regulatory standards motivates an understanding of the distribution and sources of NO₂ through observations and simulations. The TRACER-AQ campaign, conducted in Houston, TX in September 2021, provided a unique opportunity to compare observed NO₂ columns from ground-, airborne-, and satellite-based spectrometers. In this study, we investigate how these observational datasets compare, and simulate column NO₂ using WRF-CAMx with fine resolution (444 x 444 m²) comparable to the airborne column measurements. We find that observations from the GEOCAPE Airborne Simulator (GCAS) instrument were strongly correlated ($r^2=0.80$) to observations from Pandora spectrometers with a negligible bias (NMB=0.1%). Remote-sensing observations from the TROPOMI instrument were generally well correlated with Pandora observations ($r^2=0.73$) with a negative bias (NMB=-22.8%). We intercompare different versions of TROPOMI data and find similar correlations across three versions but slightly different biases (from -22.8% in v2.4.0 to -18.2% in the NASA MINDS product). Compared to Pandora observations, the WRF-CAMx simulation had reduced correlation ($r^2=0.34$) and a low bias (-25.5%) over the entire study region. We find particularly poor agreement between simulated NO₂ columns and GCAS-observed NO₂ columns in downtown Houston an area of high population and roadway densities. These findings point to a potential underestimate of vehicle NO_x emissions in the WRF-CAMx simulation driven by the Texas state inventory; and further investigation is recommended.

30



1 Introduction

Nitrogen dioxide (NO₂) is a critical precursor to criteria air pollutants (i.e., ozone or “O₃” and fine particulate matter or “PM_{2.5}”) that are above regulatory thresholds in many urban areas. Exposure to NO₂ is also directly associated with asthma exacerbation in vulnerable groups (Achakulwisut et al., 2019; Anenberg et al., 2022) and premature death (Huang et al., 2021). Due to its short atmospheric lifetime (de Foy et al., 2014), observations of NO₂ can reveal fine-scale patterns associated with sources. A major source of NO₂ is fossil-fuel combustion (McDuffie et al., 2020) and in many urban airsheds this is the dominant contributor to NO₂; however, other natural sources – like lightning (Murray, 2016) and soil microbes (Hudman et al., 2012) – along with fires (Jin et al., 2021) and tropospheric-stratospheric NO₂ exchange also contribute to NO₂ levels. The health burden, sources, and short atmospheric lifetime of NO₂ all compound in urban environments where there are large populations, diverse contributors, and unique fine-scale patterns in NO₂ levels.

In the US city of Houston, Texas – the fifth most populous metropolitan region in the US (United States Census Bureau, 2022) – NO₂ pollution is a major concern (Mazzuca et al., 2016). The large petrochemical industry in Houston emits NO₂ in addition to other common heavy emitting sources associated with coastal urban environments like vehicles, power stations, and shipping channels (Kim et al., 2011). The co-location of this large population with high levels of NO₂ presents a major public health concern that motivates research to better understand the sources that are most culpable in contributing to air pollution. Major highways like the I-610 interstate, the I-10 interstate, and Beltway 8 have heavy vehicle traffic that are responsible for elevated NO₂ concentrations (Miller et al., 2020). Large power stations and industrial facilities operate within and around the Houston metropolitan area and these point sources – along with a large shipping channel – are responsible for NO₂ plumes (Luke et al., 2010). Characterizing the unique imprints of these disparate sources remains a question of scientific concern. There is also evidence that low-income and non-white populations in Houston are disproportionately affected by air pollutants such as NO₂ (Demetillo et al., 2020).

Synchronous observations of NO₂ column densities from aircraft, ground-based, and satellite spectrometers coincided in September 2021 during the Tracking Aerosol Convection interactions ExpeRiment– Air Quality (TRACER-AQ). This campaign provided a unique opportunity to investigate the fine-scale patterns in NO₂ levels in Houston, TX. One of the devices employed during the TRACER-AQ campaign across its twelve flight days was the Geostationary Coastal and air pollution events Airborne Simulator (GCAS) instrument that has been discussed in many previous studies (e.g., Judd et al., 2020; Kowalewski & Janz, 2014; Leitch et al., 2014; Nowlan et al., 2018). The GCAS instrument is a UV-VIS spectrometer. Its data is used to retrieve NO₂ columns over a limited number of flight days; this made its observational average more sensitive to meteorological conditions than an instrument with a longer time-record; however, this tool observes NO₂ patterns with uniquely fine-scale resolution (on average 560 x 250 m²) and performed comprehensive measurements of NO₂ columns across large swaths of the city repeatedly up to three time per day. This differs with observations from the TROPOMI instrument on board the Copernicus Sentinel-5 Precursor (S5P) satellite that is in a near-polar sun synchronous orbit (van Geffen et al., 2022) that only



70 observes NO₂ once per day in the early afternoon at a coarser resolution of 3.5 x 5.5 km² at nadir. TROPOMI and
GCAS spectra are used to retrieve slant NO₂ columns that are converted into vertical columns using an air mass
factor (AMF) (Palmer et al., 2001) which is the largest source of uncertainty in the tropospheric vertical column
retrieval algorithm (Lorente et al., 2019). Comparing TROPOMI data to other observations – like those from aircraft
or ground-based monitors – can serve as a useful diagnostic in characterizing its performance and potential biases.
These characterizations have large-scale implications since TROPOMI measures NO₂ columns globally and is
75 useful in areas that lack the observational infrastructure of other instruments. The Pandora Global Network (PGN)
is a network of Pandora instruments (Herman et al., 2009); these instruments are UV-VIS spectrometers that
measure spectrally resolved radiance data that is used to retrieve total vertical NO₂ columns. A total of seven
Pandora instruments were operational during the TRACER-AQ campaign across three separate sites in and around
downtown Houston.

80 The Comprehensive Air Quality Model with Extensions (CAMx) is a multi-scale photochemical model that can
simulate air pollutants including ozone, fine particulate matter, and NO₂ (Ramboll, 2022b). CAMx has been used
extensively to investigate Texas air quality by leveraging model input data created by the TCEQ for air quality
planning (Ge et al., 2021; Goldberg et al., 2022) with strong performance compared to remote-sensing column
85 concentrations in Texas (Goldberg et al., 2022; Li et al., 2023; Soleimanian et al., 2023). CAMx can be coupled with
meteorological models like the Weather Research and Forecasting Model (WRF) which provide the meteorological
inputs necessary to simulate fine-scale atmospheric conditions (Jia et al., 2017) – this coupled modeling system is
denoted as WRF-CAMx. Fine-scale simulations from WRF-CAMx are useful to understand biases in simulated NO₂
and to identify under- or over-estimates of emissions from sectors and regions in the inventories that drive the
90 model.

In this study, we leverage the unique coincidence of ground-based Pandora spectrometers, high-resolution airborne,
and TROPOMI-based remote sensing observations of column NO₂ during the September 2021 TRACER-AQ
campaign. We assess the capabilities of these different data sources through cross-comparisons then compare
95 observed NO₂ to simulated values from a WRF-CAMx simulation to evaluate its performance. Additionally, we
consider the impact of different TROPOMI algorithms on performance against Pandora measurements. Our
comparisons across the three observational datasets clarifies the range of expected values of NO₂ column
concentrations in Houston, TX and characterizes potential deficiencies and biases in observational products and
simulated CAMx values. We investigate weekday-weekend performance of the model and consider differences in
100 the spatial distributions of NO₂ columns to qualitatively identify the sources that may be under- or overestimated in
local inventories and identify the regions in Houston that are most likely impacted by these incorrectly attributed
emissions. Additionally, we compare diurnal profiles in column and surface concentrations of NO₂ across relevant
products.



2 Data and Methods

105 2.1 Pandora Observations

During the TRACER-AQ campaign a total of seven Pandora instruments operated across three sites in Houston (Table 1). Pandora instruments are ground-based UV-VIS spectrometers that measure spectrally resolved radiances and this work only utilizes those collected via direct-sun observations (Herman et al., 2009). Trace gas spectral fitting routines are employed to characterize column concentrations of gases (e.g., NO₂) similar to remote-sensing and aircraft observations (Judd et al., 2020). Details on the Pandora instruments and their fitting routines are discussed in detail in past studies (Cede, 2021; Herman et al., 2009). The study was designed to have two Pandoras operating at once during the study. However, this analysis only uses data from a single Pandora at each site. This avoids unevenly weighting coincidences that would arise from intercomparisons with airborne, TROPOMI and CAMx datasets. Pan #59 at Aldine, #61 at La Porte, and #25 and University of Houston were chosen for the following reasons. As indicated in Table 1, Pan #61 and Pan #58 clearly have the largest temporal coverage during the TRACER-AQ time period. While Pan #188 measured more frequently at the University of Houston than Pan #25, Pan #188 was operated on a tower about 70 meters above the surface, which results in missing portions of the tropospheric column when operated in direct-sun mode.

120 Locations of the three sites are presented in Fig. 2F. These three chosen sites are shaded and bolded in the table below. Pandora direct-sun retrievals represent the “total vertical column” of NO₂ which differs from the aircraft measurements that only measure the tropospheric column. We directly compare these disparate sources by adding a “stratospheric NO₂ column component” derived from TROPOMI estimates to the aircraft measurements (see section 2.2 and 2.3) to compare total column amounts.

125

Table 1: Details on Pandora instrument operational time

Inst. #	Location	Lat.	Lon.	September 2021 Flight Days with Observations (Number of high- and medium-quality measurements per day)									
				1 st	3 rd	8 th	9 th	10 th	11 th	23 rd	24 th	25 th	26 th
11	La Porte	29.67	-95.06	322	347	0	0	0	0	0	0	0	0
58	La Porte	29.67	-95.06	132	190	412	319	415	362	92	439	414	401
63	La Porte	29.67	-95.06	0	0	0	0	0	0	0	0	265	207
61	Aldine	29.90	-95.33	168	253	400	391	419	367	420	420	405	420
148	Aldine	29.90	-95.33	5	1	3	1	3	3	17	17	10	17
25	U of H	29.72	-95.34	213	256	300	299	392	273	400	382	400	344
188	U of H	29.72	-95.34	528	610	1184	957	1137	722	372	749	225	95



2.2 GCAS Observations

130 The GCAS instrument was installed on the NASA G-V aircraft. The GCAS instrument employs charge-coupled
 device array detectors to observe backscattered light. These data can be used to retrieve column densities of gases
 like NO₂ below the aircraft using a DOAS computing software (Danckaert et al., 2017). During TRACER-AQ,
 GCAS collected data over the Houston metropolitan area across 12 days during late August and throughout
 135 September 2021. The flight strategy of the aircraft included flying the plane in a ‘lawnmower’ fashion with flight
 lines spaced 6.3 km apart, ensuring overlap at flight altitude (FL280) with the instrument field of view of 45 degrees
 creating one gapless map of NO₂ up to three times per flight day. NO₂ observations from GCAS are publicly
 available at the NASA Atmospheric Sciences Data Center (NASA/LARC/SD/ASDC, 2022). Observations from two
 of the flight days – a test flight (August 30) and a flight over the Gulf of Mexico (September 27) are excluded from
 this study because they provided no meaningful data over Houston. Given the relatively short timeframe of flight
 data collection; meteorological conditions have an influence on the fine-scale patterns in NO₂ columns observations.
 140 Owing to this, we summarize some basic conditions and information of the 10 flight days that focused on Houston
 (Table 2). Wind and meteorological conditions were determined by review of historical weather archives taken at
 Houston Hobby Airport (NASA, 2023; Weather Underground, 2023).

Table 2: Basic meteorological conditions and notes during GCAS flights

145

Day of Sept 2021	Day of the Week	High Temp	Wind direction	Additional note
1	Wed	96 F	Weak SW winds	Thunderstorms from S to N, 11 AM to 4 PM
3	Fri	93 F	Weak S winds	Scattered thunderstorms 12 PM to 4 PM
8	Wed	94 F	N turning NE	Clear skies and no rain
9	Thurs	95 F	N turning NE	Afternoon fair weather clouds, no rain
10	Fri	93 F	NE turning E	Clear skies, no rain, some long-range smoke aloft
11	Sat	93 F	E winds	Afternoon fair weather clouds, no rain
23	Thurs	83 F	E winds	Clear skies, no rain, cold front overnight Sept 21
24	Fri	84 F	E turning SE	Clear skies, no rain
25	Sat	87 F	NE turning E	Clear skies, no rain
26	Sun	83 F	Calm then SE	Clear skies, afternoon fair weather clouds

The publicly available GCAS measurements (version R2) include a version of the dataset with reprocessed AMFs to include NO₂ vertical profile estimates from the fine-scale (444 × 444 m²) WRF-CAMx simulation used in this



analysis (section 2.4). Air mass factors use this vertical profile information to account for altitude-dependent sensitivities in remote-sensing observations. The original vertical profiles in the publicly available dataset were derived from a global model, GEOS-CF (Keller et al., 2021), that had a coarser spatial resolution ($0.25^\circ \times 0.25^\circ$). Lastly, to directly compare GCAS measurements to other NO_2 column concentrations we regrid them to a common grid; in this study, we chose the fine-scale WRF-CAMx grid. Only cloud-free GCAS data is considered in this analysis.

To characterize the accuracy and precision of GCAS measurements we compare them to observations from the Pandora instruments (section 3.1). This comparison requires both spatial and temporal screening. Spatially, we identify the CAMx grid cell in which each Pandora instrument is located and only consider GCAS measurements that were regridded to these grid cells. Temporally, we screen out all Pandora measurements that are more than 15 minutes removed from a GCAS overpass and then identify the Pandora measurement time within this 30-minute window that most closely matches the GCAS overpass time. After screening the data, we also account for the fact that GCAS only measures the tropospheric component of the NO_2 column. There is a substantial but predictable “above-aircraft” column that is not reflected in the GCAS measurements. This is primarily associated with stratospheric NO_2 . To account for this, we approximate the above aircraft component of the GCAS NO_2 columns using the stratospheric NO_2 column component of TROPOMI measurements (section 2.3) and add this bias correction factor to GCAS observations.

2.3 TROPOMI Observations

The TROPOMI instrument – on board the Sentinel-5P satellite – has measured total slant columns of NO_2 daily at approximately 1:30 PM local time globally from April 30, 2018 to present (European Space Agency, 2021). The slant column measurements are converted into tropospheric vertical column amounts by subtracting off a stratospheric NO_2 component and transforming the remaining tropospheric slant column to vertical column using an air mass factor. We download the publicly available data (<https://data-portal.s5p-pal.com/products/no2.html>) coincident with the TRACER-AQ campaign in September 2021 for overpasses of Houston, TX. In this study, we primarily consider measurements from the latest version (2.4.0) (Eskes et al., 2023); however, we additionally consider measurements processed using the version 2.3.1 algorithm (van Geffen et al., 2021) and the NASA Multi-Decadal Nitrogen Dioxide and Derived Products from Satellites (MINDS) product (Lamsal et al., 2022) and intercompare these different versions (Fig. 3). All product versions stem from the same slant column retrieval but differ in the calculation of the air mass factor for slant to vertical column conversions, and in the case of NASA MINDS, separation of the stratosphere and troposphere (Bucsela et al., 2013). The main difference between 2.3.1 and 2.4.0 is the use of the $0.125^\circ \times 0.125^\circ$ Directional Lambertian Equivalent Reflectivity (DLER) climatology derived from TROPOMI observations which replaces an old $0.5^\circ \times 0.5^\circ$ Lambertian Equivalent Reflectivity (LER) dataset used in v2.3.1 (Eskes et al., 2023). NASA MINDS uses a geometry-dependent surface Lambertian Equivalent Reflectivity (GLER) product for their surface reflectivity input into the AMF calculation based on



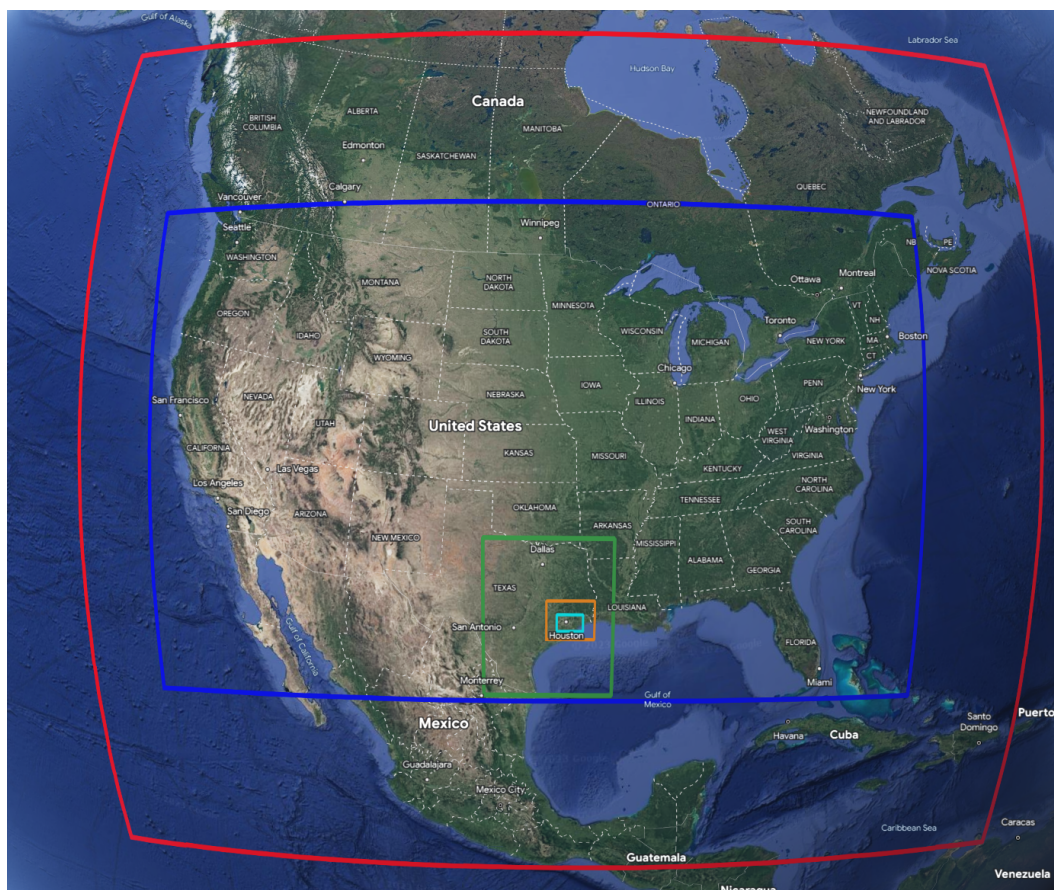
185 MODIS observations. The other main difference in these products include use of different a priori NO₂ profiles (1° × 1° TM5-MP for v2.3.1 and v2.4.0 vs 0.25° × 0.25° GMI simulation for NASA MINDS). A comparison between TROPOMI version 2.4.0 and a MAX-DOAS network found that in moderately polluted locations, TROPOMI had a median bias of -35% (Lambert et al., 2023).

These publicly available TROPOMI data are further processed for this study. We screen TROPOMI measurements to consider cloud coverage and erroneous data using the recommended qa_value filter (> 0.75). We regrid the
190 TROPOMI NO₂ observations (resolution of 3.5 × 5.5 km² at nadir) onto the WRF-CAMx grid (444 × 444 m²). When comparing TROPOMI observations to Pandora instruments we follow the same spatial and temporal screening approach as discussed for GCAS. Spatially, we identify the CAMx grid cell in which each Pandora instrument is located and only consider TROPOMI measurements that were regridded to these grid cells. Temporally, we screen out all Pandora measurements that are more than 15 minutes removed from a TROPOMI
195 overpass and then identify the Pandora measurement time within this 30-minute window that most closely matches the TROPOMI overpass time. Using WRF-CAMx vertical profile information we calculate both a total and tropospheric NO₂ column from TROPOMI measurements and we difference the total and tropospheric values to calculate a stratospheric NO₂ column component from TROPOMI. We take the spatial and temporal average of this stratospheric component in Houston during the TRACER-AQ campaign to calculate a constant bias correction to
200 convert tropospheric NO₂ columns – from GCAS and WRF-CAMx – to quasi-total NO₂ columns when comparing them to total NO₂ column measurements from Pandora instruments.

2.4 WRF-CAMx simulated NO₂

For this study, a set of simulations were conducted employing version 4.3.3 of the Advanced Research Weather Research and Forecast (ARW) model (Skamarock et al., 2021) jointly with the Comprehensive Air Quality Model
205 with Extensions (CAMx) v7.20 with the CB6r5 chemical mechanism for a simulation period that matched the September 2021 TRACER-AQ timeframe. A new high-resolution modeling platform was designed specifically for this study that adopted prior approaches used in Texas Commission on Environmental Quality (TCEQ) state implementation plan (SIP) modeling (TCEQ, 2021) to update emissions.

210 The WRF model is a mesoscale numerical weather prediction system designed to serve both operational forecasting and atmospheric research needs (Skamarock et al., 2005, 2008). We define the WRF modeling domains as slightly larger than the corresponding CAMx domains (Fig. 1) to avoid possible numerical artifacts near domain boundaries when transferring WRF meteorology to CAMx. The 36 km CAMx domain (red) includes the continental US, Mexico, and parts of Central America and Canada. The 36 km, 12 km (blue) and East Texas 4 km (green) domains
215 are also used by the TCEQ for State Implementation Plan (SIP) modeling. The higher resolution domains (1.333km (orange) and 0.444km (cyan)) were selected to include the most relevant GCAS flight tracks while considering computational expense.



220

Figure 1: Modeling domains used in the CAMx simulation for the 36 km resolution (red), 12 km resolution (blue), 4 km resolution (green), 1.333 km resolution (orange), and the 0.444 km resolution (cyan). Maps data provided by Google © 2020, Landsat / CopernicusData SIO, NOAA, U.S. Navy, NGA, GEBCO, IBCAO, INEGI, and U.S. Geological Survey.

225 Additional information on the WRF-CAMx modeling is included in the supplemental including the WRF physics options (Table S1), vertical layer mapping from WRF to CAMx (Table S2), and CAMx science options (Table S3). We used 0.25° Global Forecasting System (GFS) data assimilation system (GDAS) analysis data (DOC/NOAA/NWS/NCEP/EMC, 2023) as initial conditions for the WRF meteorological model; this GDAS data is also used for boundary conditions and data assimilation. We configured the output timesteps of WRF to 15 minutes

230 for the higher resolution domains. The CAMx simulation was first performed over the coarser domains (36 km, 12km, and 4 km) from which initial and boundary conditions were extracted for the higher resolution domains. TCEQ developed the 2019 modeling emissions inventory for the Dallas-Fort Worth (DFW) and Houston-Galveston-



Brazoria (HGB) Reasonable Further Progress (RFP) SIP revision (TCEQ, 2021). Starting with this inventory we implement further changes as discussed in the next paragraph.

235

First, we update the CAMx modeling emissions inventory from the TCEQ platform to incorporate 2021 hourly Continuous Emissions Monitoring Systems (CEMS) (EPA, 2023) data for the eleven major EGUs listed in Table S4. We download hourly data from Clean Air Markets Division (CAMPD) for the eleven EGUs for the August 30-Sep 27, 2021, period and stack parameters were based on the TCEQ 2019 emissions platform (TCEQ, 2021). Second, we

240

update shipping emissions to incorporate MARINER v2 (Ramboll, 2022a) emissions built with 2021 Automatic Identification System (AIS) data for the higher resolution domains. Third, we reprocess link-based on-road mobile emissions for the higher resolution domains. Fourth, we update biogenic emissions and lightning NO_x based on WRF meteorology. Specifically, we use the Model of Emissions of Gases and Aerosols from Nature (MEGAN) (Guenther et al., 2012) version 3.2 for biogenic emissions, the Fire Inventory of NCAR (FINN) version 2.2

245

(Wiedinmyer et al., 2011) for fire emissions, and lightning NO_x emissions derived by applying the CAMx LNO_x processor² to the 2021 meteorological data from the WRF simulation. Considering the limited extent of the high-resolution CAMx domains and large degree of uncertainty with both the fire and LNO_x emissions, we excluded these two emission sources from the finer resolution domains. Lastly, we regrid all other gridded emissions from the coarser domains to the high-resolution domains without refining their spatial resolution. Daily emissions of NO_x and VOC in tons per day (tpd) for a September weekday are presented in Table 3 below.

250

Table 3: CAMx 444 × 444 m² domain-wide summary of average September weekday emissions by sector in units of tons per day (tpd).

Emission Sector	NO _x (tpd)	VOC (tpd)
EGUs	25.5	0.2
On-road mobile	70.9	34.7
Railyards	4.2	0.3
Shipping	63.9	4.3
KIAH airport	6.4	0.8
KHOU airport	1.8	0.4
Other		
Off-road mobile*	33.1	31.4
Non-EGU Point Sources	47.9	27.8
Oil and Gas	0.2	0.0
Area	92.8	623.2
MEGAN biogenic	25.9	319.7



2.5 Diurnal Comparison

We further intercompare these data by grouping them at locations and then calculating their average diurnal profiles during the TRACER-AQ campaign for both column and surface-level NO₂. Specifically we compare GCAS, CAMx, Pandora, and GEOS-CF (Keller et al., 2021) NO₂ columns at the three Pandora sites during TRACER-AQ flight days. Simulated surface and NO₂ columns from GEOS-CF are obtained through the GMAO OPeNDAP interface (<https://opendap.nccs.nasa.gov/dods/>) for all of 2021 and filtered to the specific Pandora instrument locations and during TRACER-AQ flight days. We apply both spatial and temporal screening. Spatially, we identify the CAMx grid cell – for GCAS and CAMx – and GEOS-CF grid cell in which the Pandora instrument is located. Temporally, for GCAS, we round all overpass times to the nearest hour and calculate the median value for each hour across all overpasses and days. For CAMx, GEOS-CF, and Pandora we identify the simulated and observed NO₂ column concentration closest to the hour and calculate the median value across all flight days and locations.

For diurnal comparisons at the surface, we use surface-level NO₂ concentrations from CAMx and GEOS-CF and apply the same temporal screening. Spatially, for the surface-level we consider concentrations at a point in between the three Pandora instruments that is representative of downtown concentrations (29.7 °N, 95.3 °W). We choose this point to represent the temporal behavior of the wider regions rather than individual sites. Additionally, we download hourly NO₂ concentrations from the US Environmental Protection Agency (EPA) Air Quality System (AQS) (https://aqs.epa.gov/aqsweb/airdata/download_files.html). We download all hourly data for 2021 for the US and filter the TRACER-AQ flight days and for monitors in Harris County. We identify the median hourly concentrations across these monitors and the TRACER-AQ flight days.

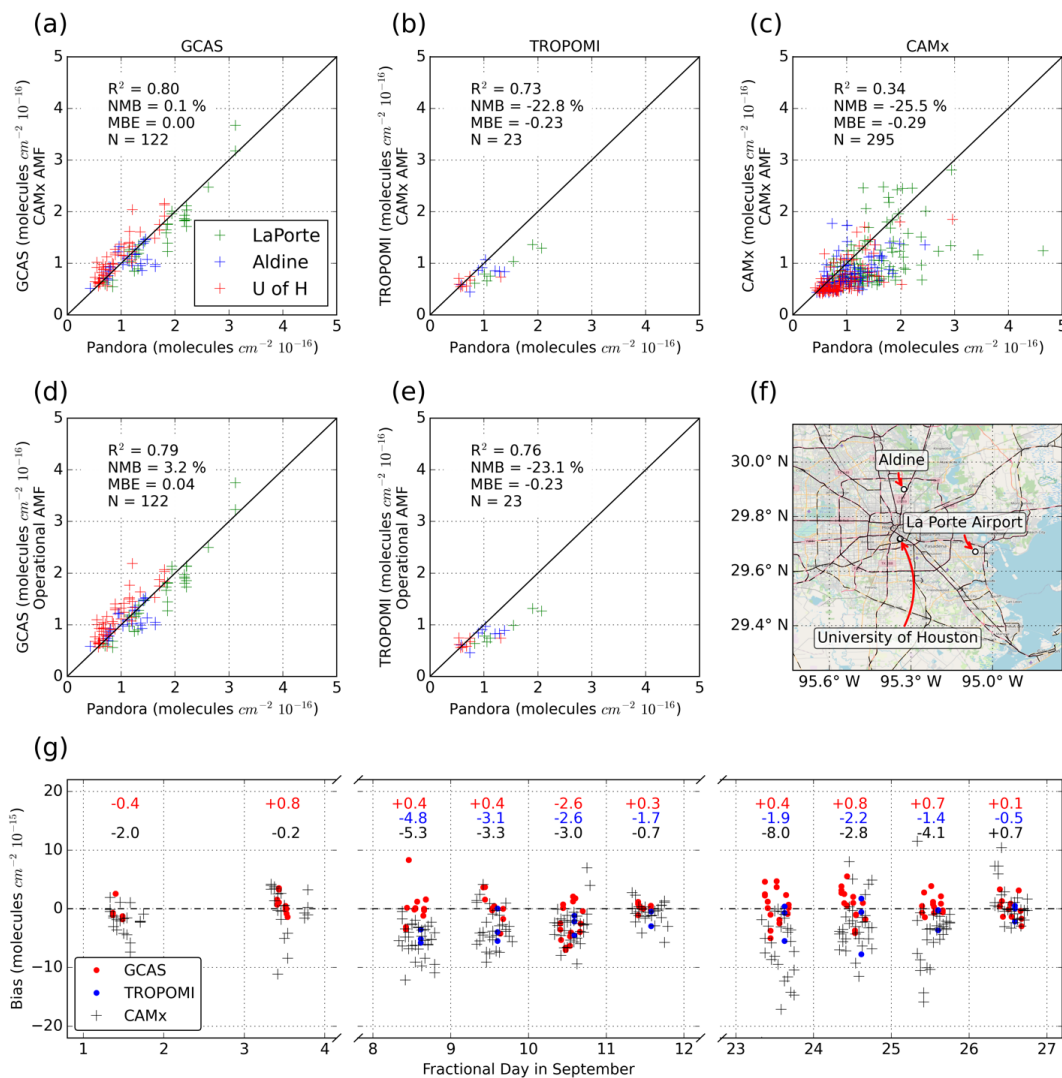
3 Results

3.1 Comparisons to Pandora Observations

The observations from ground-based Pandora instruments are considered the most accurate of all observational platforms presented in this project due to low uncertainties in their air mass factors (Herman et al., 2009) when operating in direct-sun mode. The air mass factor in this mode is calculated from simple solar geometry – unlike TROPOMI and GCAS, which rely on *a priori* assumptions like the vertical NO₂ profile and surface reflectivity. Given this, we use Pandora observations as our reference dataset to characterize the performance of the two observational datasets – GCAS and TROPOMI – along with the WRF-CAMx simulation across three sites (Table 1). These three sites (Aldine, La Porte, and University of Houston) are located in the heavily polluted inner region of Houston that we denote as “urban Houston” (Fig. 2F). Background observations from Pandora instruments in less polluted sites were unavailable during the TRACER-AQ campaign so there is less certainty about the performance of GCAS, TROPOMI, and CAMx outside of urban Houston. We consider the performance of GCAS processed with a CAMx-based AMF (Fig. 2A), TROPOMI processed with a CAMx-based AMF (Fig. 2B), and CAMx (Fig. 2C)



and the performance of GCAS and TROPOMI with the operational AMFs (Fig. 2D and 2E) individually and then intercompare the three datasets across the ten GCAS observation days (Fig. 2G).



290

Figure 2: Comparison of Pandora total column NO₂ to GCAS using CAMx-based AMFs (A), TROPOMI v2.4.0 using CAMx-based AMFs (B), and CAMx (C) and GCAS (D) and TROPOMI v2.4.0 (E) with their operational AMFs. Tropospheric columns from GCAS and CAMx are bias corrected with a TROPOMI-derived stratospheric column factor as discussed in the methodology. Data from all possible overpasses coincident within 15 minutes of a Pandora observation are considered. GCAS flight times generally ranged from 8:00 AM-4:00 PM CDT. TROPOMI overpasses occurred around 1:30 PM local time. Color coding

295



indicates which of the Pandora instruments NO₂ column concentrations are being compared against indicated
in the legend in subplot A, but statistics are presented across all locations. Map of Pandora instrument sites in
urban Houston (F). Bias between the three datasets and Pandora across GCAS flight days (G) with the
300 overall average daily bias indicated above the points for all three datasets. The data are color coded based on
the observed or simulated source that is being compared against Pandora measurements. © OpenStreetMap
contributors 2023. Distributed under the Open Data Commons Open Database License (ODbL) v1.0.

In Fig 2A-C we characterize the performance of the observational and simulated datasets of NO₂ column
305 concentrations across the three sites in Houston. For each of the GCAS flight days, we compare GCAS and
TROPOMI observation against Pandora measurements for every overpass that was not obstructed by cloud
coverage; for CAMx we compare simulated columns for every daytime hour of each GCAS flight day.

Observations from GCAS were both well correlated ($r^2=0.80$ and minimally biased (NMB=+0.1%) when compared
310 to measurements from Pandora. Use of the CAMx AMF in place of the operational AMF had a negligible impact on
comparisons to Pandora (from $r^2=0.79$ and NMB=+3.2%). Observations from TROPOMI on GCAS flight days were
also well correlated with Pandora measurements ($r^2=0.73$) but there was a negative bias (NMB=-22.8%) in v2.4.0.
This bias was worse for more NO₂ polluted scenes. Similar to GCAS, observations from TROPOMI were slightly
affected by the new CAMx AMF (from $r^2=0.76$ and NMB=-23.1%) with a slight degradation in correlation and
315 slight improvement in bias. This negative bias may be attributable to the coarser resolution of TROPOMI compared
to GCAS that weakens its ability to capture fine-scale plumes (Wagner et al., 2023) of NO₂ associated with road
systems, airports, power stations, and industrial facilities.

We calculate the ratios of the TROPOMI v2.4.0 product with the CAMx AMF compared to the operational AMF
320 (Fig. S1) in September throughout the domain and note that the areas with Pandora instruments – in urban Houston
– have equivalent values; however, in rural areas the CAMx AMF has a greater impact on TROPOMI NO₂ columns.
Given that Pandora instruments were not located at either the most or least polluted areas of the metropolitan area,
the benefit of the CAMx AMF may be underrepresented by our findings at the Pandora sites.

We compare simulated NO₂ columns from CAMx with Pandora measurements; however, in this comparison there
are more points to intercompare as columns were simulated for each hour of every flight day by CAMx and
observed multiple times per hour from Pandora. The CAMx simulated columns were less correlated with Pandora
measurements ($r^2=0.34$) than compared to TROPOMI and GCAS, and they had a consistent negative bias (NMB=-
25.5%). This poor correlation could partially be explained by differences in WRF simulated meteorology and
330 observed meteorology specifically from differences in wind speed and direction and an inability to capture the bay
breeze in Houston. The negative bias is likely attributable to an underestimate of NO_x emissions, but it could also be
partially due to an incorrect effective NO₂ lifetime driven by the nonlinear interactions of chemistry and dispersion.



Additionally, there can be substantial differences in vertical mixing coefficients in different schemes in the models, and these can impact the biases in column concentrations (de Foy et al., 2007; Riess et al., 2023).

335

In Fig. 2G, we intercompare the daily variability in biases across the ten GCAS flight days. There were no TROPOMI data for the first two flight days because cloud coverage blocked TROPOMI observations at the Pandora sites during its overpass time. The daily average bias of GCAS observations were consistently small throughout the entire period: they ranged from -2.6 to +0.8 molecules $\text{cm}^{-2} 10^{15}$ on September 10th and the 3rd and 24th, respectively.

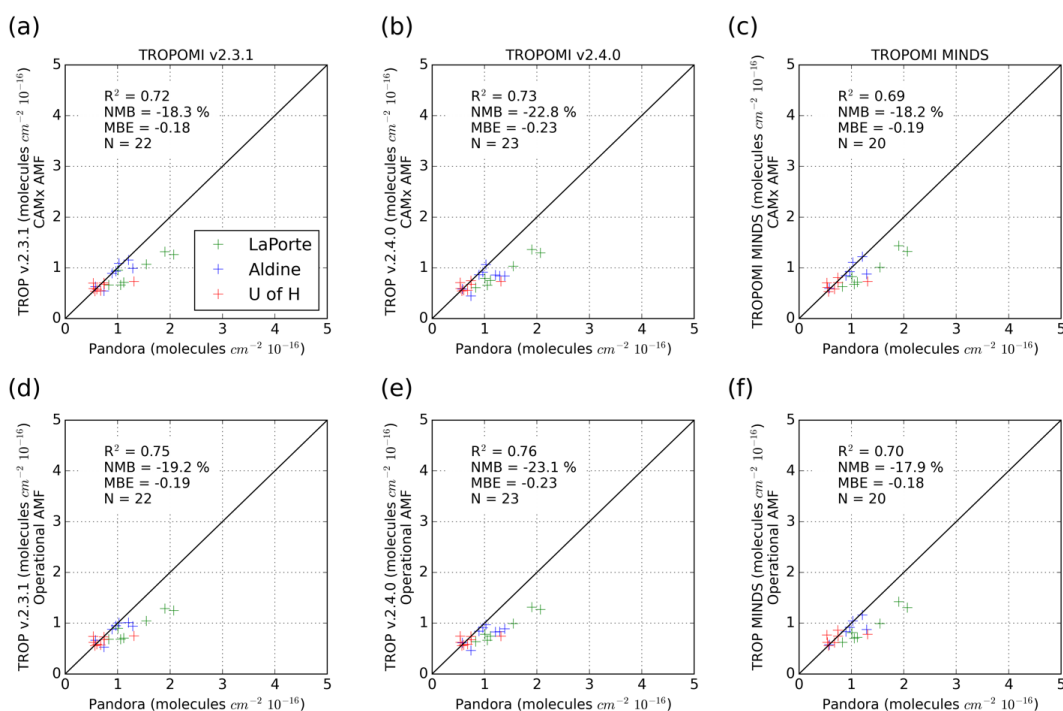
340

TROPOMI observations were consistently biased systematically low: they ranged from -4.8 to -0.5 molecules $\text{cm}^{-2} 10^{15}$; however, on all days except the 26th daily averaged TROPOMI biases were more negatively biased than -1.3 molecules $\text{cm}^{-2} 10^{15}$ compared to Pandora measurements. Unlike the two observational datasets, the bias in simulated CAMx NO₂ columns had much higher daily variability. On some days, such as September 3rd, there was little bias in simulated columns compared to Pandora measurements, and on other days such as September 26th, there

345

was a minor high bias (+0.7 molecules $\text{cm}^{-2} 10^{15}$); however, on most days there was a negative bias that was the strongest on September 23rd when NO₂ columns were biased as low as -8.0 molecules $\text{cm}^{-2} 10^{15}$. Generally, simulated CAMx columns perform better on weekend days (11th, 25th, and 26th) which is investigated in greater detail in section 3.4.

3.2 Comparisons of different TROPOMI algorithms to Pandora Observations



350



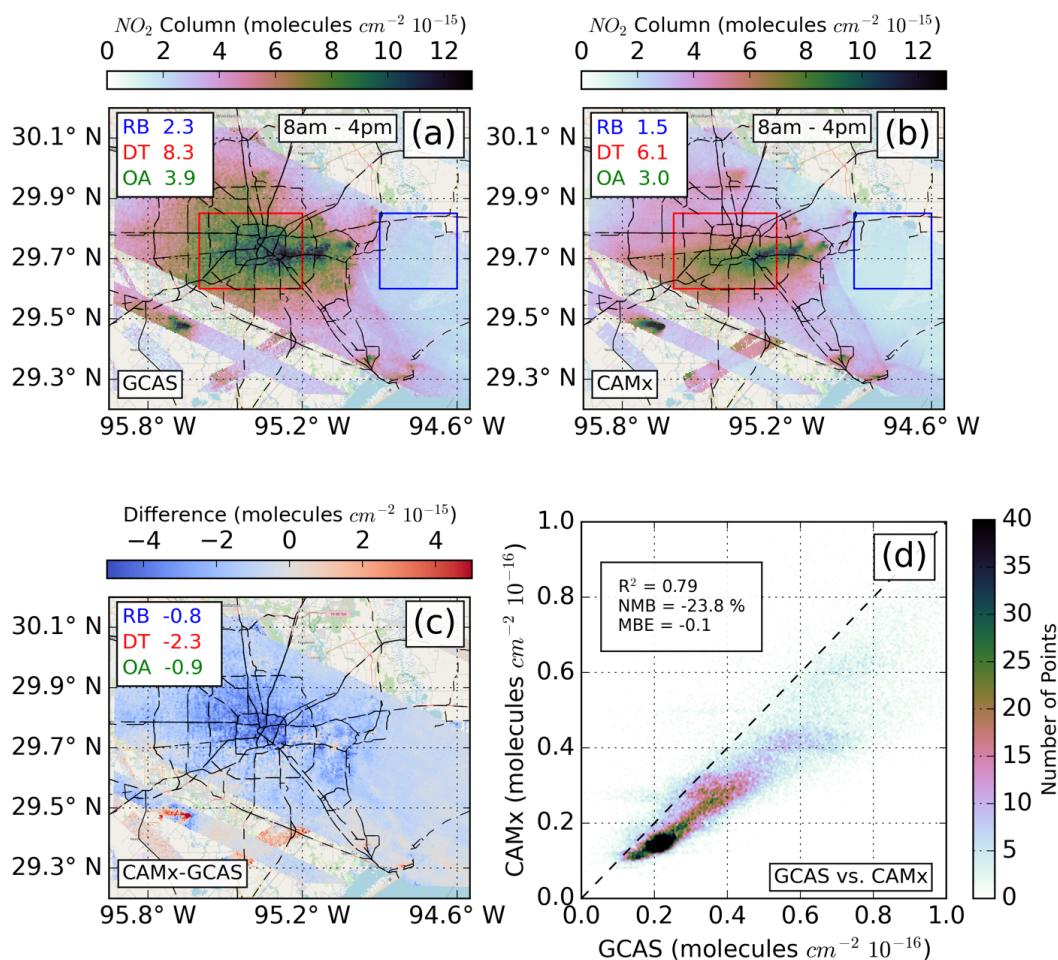
Figure 3: Comparison between Pandora measurements and TROPOMI observations using the CAMx AMF for version 2.3.1 (A), 2.4.0 (B), and NASA MINDS (C) and the same respective versions using the operational AMF (D-F). Data from all possible overpasses coincident within 15 minutes of a Pandora observation are considered with one exception: data from September 11th, 2021, was missing from the NASA MINDS product and so values in plots C and F exclude this day.

We intercompare TROPOMI observations to Pandora measurements across three different algorithms: version 2.3.1 (Fig. 3 A, D), version 2.4.0 (Fig. 3B, E), and the NASA MINDS product (Fig. 3C, F) using both the CAMx AMF (top row) and the Operational AMF (bottom row) for the same Pandora instruments in Houston during the TRACER-AQ Campaign. Overall, the choice of algorithm and AMF does affect the performance of TROPOMI compared to Pandora, albeit slightly. Regardless of AMF, version 2.4.0 appears to have the worst normalized mean bias in Houston during TRACER-AQ ($r^2=0.73$, and $NMB=-22.8\%$), version 2.3.1 is improved ($r^2=0.72$ and $NMB=-18.3\%$) while the NASA MINDS product performs comparably ($r^2=0.69$ and $NMB=-18.2\%$) to version 2.3.1. Notably, NASA MINDS data for September 11th are missing so these data are excluded from panels C and F. For version 2.3.1 and version 2.4.0 the CAMx AMF slightly improves the bias; however, for the MINDS product the CAMx AMF slightly worsened bias compared to the operational AMF. The correlation is generally unaffected by the choice of AMF. We choose TROPOMI version 2.4.0 for the intercomparison in the following sections as it is the most recent version.

3.3 Comparisons of GCAS, TROPOMI, and CAMx data on the CAMx grid

The comparisons between Pandora measurements and the datasets indicate that GCAS observations are in best agreement with Pandora. While TROPOMI performs worse than GCAS, it still decisively outperforms simulated NO_2 columns from CAMx at Pandora sites in both correlation and bias despite its coarser resolution. With the above in mind, in this section we present NO_2 columns observed from GCAS and TROPOMI and simulated from CAMx at the $444 \times 444 \text{ m}^2$ resolution of the CAMx grid. We extend the prior comparison beyond focusing on three discrete points in urban Houston to the entire CAMx domain to get a more complete picture of the spatial components of these datasets. For each dataset we consider observations across all ten GCAS flight days. We begin by comparing GCAS observations only with CAMx simulated columns across all GCAS overpasses as these data are less limited temporally than TROPOMI observations (Fig. 4).

380



385 **Figure 4: Comparison of GCAS observations to CAMx simulated NO₂ columns across all data during GCAS overpasses (generally 8 am – 4 pm). Temporally averaged GCAS NO₂ columns (A), temporally averaged simulated CAMx NO₂ columns (B), the absolute difference between GCAS and CAMx (C), and a scatter density plot comparing all observations between GCAS and CAMx (D). We identify three distinct areas: downtown or “DT” (red), the low emissions East Galveston rural Bay or “RB” (blue), and all other areas or “OA” (green) and calculate the averages in the top left of each chart. © OpenStreetMap contributors 2023. Distributed under the Open Data Commons Open Database License (ODbL) v1.0.**

390

When considering data from all GCAS overpasses (Fig. 4A, B, C) we observe a consistent negative bias in the CAMx product compared to GCAS observations throughout the domain that worsens in the downtown (DT) area (-2.3

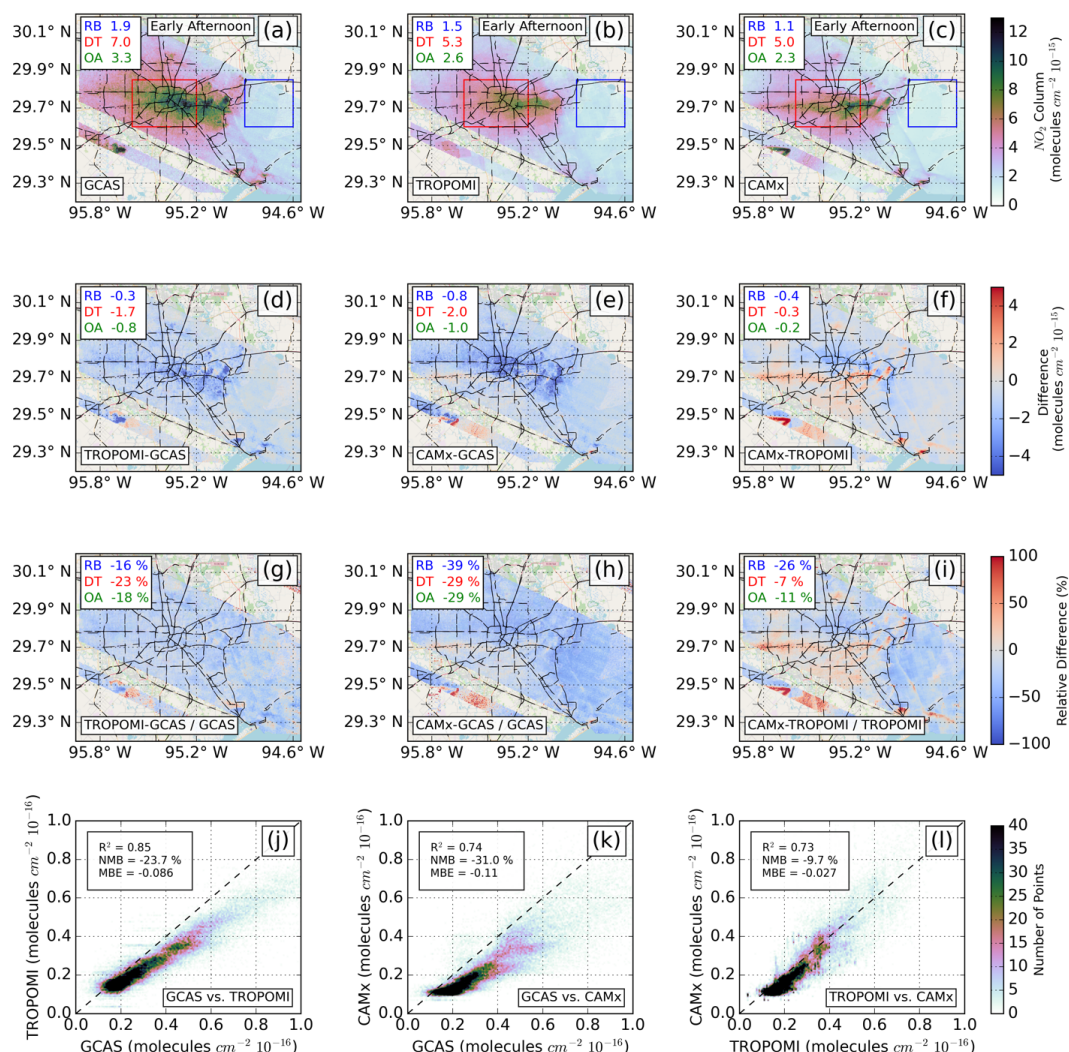


molecules $\text{cm}^{-2} 10^{-15}$) compared to background levels in the rural East Galveston Bay (RB) ($-0.8 \text{ molecules cm}^{-2} 10^{-15}$).

395 Near the W A Parish power station in the southwestern area of the domain there are a mixture of positive and negative biases in the CAMx simulated columns that are likely indicative of errors in wind speeds or directions in the CAMx simulation. Overall, the CAMx simulated columns were well correlated with GCAS observations ($r^2=0.79$) but the negative bias was substantial (NMB= -23.8%) (Fig. 4D).

400 We continue this comparison in Fig. 5 where we limit the GCAS and CAMx values temporally around TROPOMI overpasses. For Fig. 5, we screen out all observations that are ± 90 minutes from TROPOMI overpass for each day and then temporally average the observations across the GCAS flight days (Fig. 5A-C). We difference, both absolutely (Fig. 5D-F) and relatively (Fig. 5G-I), the three pairs of datasets and present them in scatter density plots (Fig. 5J-L). We focus on three regions: downtown Houston (red) (DT), the rural East Galveston Bay (blue) (RB), and

405 all other areas (green) (OA) and calculate the mean values and differences for these areas in the top left of each of the plots. The results presented in Fig. 5 are the temporal average across all flight days; however, similar figures for individual flight days are presented in the supplemental (Fig. S2-11)



410

Figure 5: Spatial distribution of GCAS (A), TROPOMI (B), and CAMx (C) NO₂ columns averaged across the ten GCAS flight days when within 90 minutes of each TROPOMI overpass representing early afternoon NO₂ columns. We identify three distinct areas: downtown or “DT” (red), the low emissions East Galveston Bay or “RB” (blue), and all other areas or “OA” (green) and calculate the averages in the top left of each chart.

415

Absolute differences between GCAS and TROPOMI (D), GCAS and CAMx (E), and TROPOMI and CAMx (F). Relative differences between GCAS and TROPOMI (G), GCAS and CAMx (H), and TROPOMI and CAMx (I). Scatter density plots of GCAS vs. TROPOMI (J), GCAS vs. CAMx (K), and TROPOMI vs. CAMx (L). © OpenStreetMap contributors 2023. Distributed under the Open Data Commons Open Database License (ODbL) v1.0.



420

First, we consider the spatial distribution of NO₂ columns from GCAS (Fig. 5A), TROPOMI (Fig. 5B), and CAMx (Fig. 5C) independently. For all three datasets, NO₂ columns are higher in downtown Houston than in the rural East Galveston Bay; generally, they are between 3.5 and 5 times as large. The two finer-resolution datasets – GCAS and CAMx – also capture NO₂ peaks associated with point sources like those from W A Parish, Texas City, and Baytown and in the Ship Channel. A map of the major point sources discussed in this work is included in the supplemental (Fig. S12). The coarser resolution of TROPOMI leads to fewer identifiable peaks associated with point sources; however, there are slightly elevated observed values near the W A Parish and Texas City power plants and the Ship Channel. Observations from GCAS and TROPOMI reveal a more diffuse peak in NO₂ columns in and around downtown Houston that includes elevated levels of NO₂ in the western part of the city. Simulated columns from CAMx, on the other hand, primarily estimate higher NO₂ values in the eastern area of downtown Houston and have lower NO₂ values in the western area of the city.

We next consider the three products compared to one another through three methods: absolute difference (Fig. 5D-F), relative difference (Fig. 5G-I), and scatter density plots (Fig. 5J-L). We intercompare these three products by isolating three sets of pairs: that is GCAS and TROPOMI, GCAS and CAMx, and TROPOMI and CAMx.

First, considering GCAS and TROPOMI, there appears to be a systematic low bias in TROPOMI observations throughout nearly the entire domain. Regardless of the spatial subset, the low bias in TROPOMI was consistent and ranged from -23% in downtown to -16% in the rural bay (Fig. 5G). In an absolute sense, on average TROPOMI was between 0.3 and 1.7 molecules cm⁻² 10¹⁵ lower than GCAS (Fig. 5D) across the three locations. Throughout the entire domain, observations from GCAS and TROPOMI were well correlated ($r^2=0.85$), but TROPOMI had an overall negative normalized mean bias of -23.7% (Fig. 5J). We note that this low bias is slightly greater than what we would expect from considering the biases of these products relative to Pandora measurements as we do in section 3.1; doing this we would expect TROPOMI to be low biased relative to GCAS by around 23%. This slight additional negative bias indicates that either the three Pandora sites are unable to capture the full extent of the negative TROPOMI bias and that TROPOMI may be lower biased outside of these sites (e.g., areas outside of downtown Houston) or that GCAS observations may be biased additionally high outside of these sites. Notably, there are a few areas surrounding point sources in the eastern area of downtown and around the W A Parish plant in which TROPOMI observes higher NO₂ columns than GCAS. This is likely attributable to the coarser resolution of TROPOMI that results in peaks of NO₂ to be spread into surrounding areas that are in the same TROPOMI grid cell.

Second, comparing GCAS to CAMx we again find a low bias relative to GCAS, albeit one with a higher degree of spatial variability. In the remote bay, CAMx simulated columns are lower than GCAS compared to elsewhere in the domain (-39%) (Figure 5H) while downtown and background levels are similarly biased at 29% in a relative sense. This lower bias in the low emission East Galveston Bay is indicative of an underestimation of background NO₂ columns in the CAMx simulation. Across these three regions the mean absolute differences range from -0.8 to -2.0

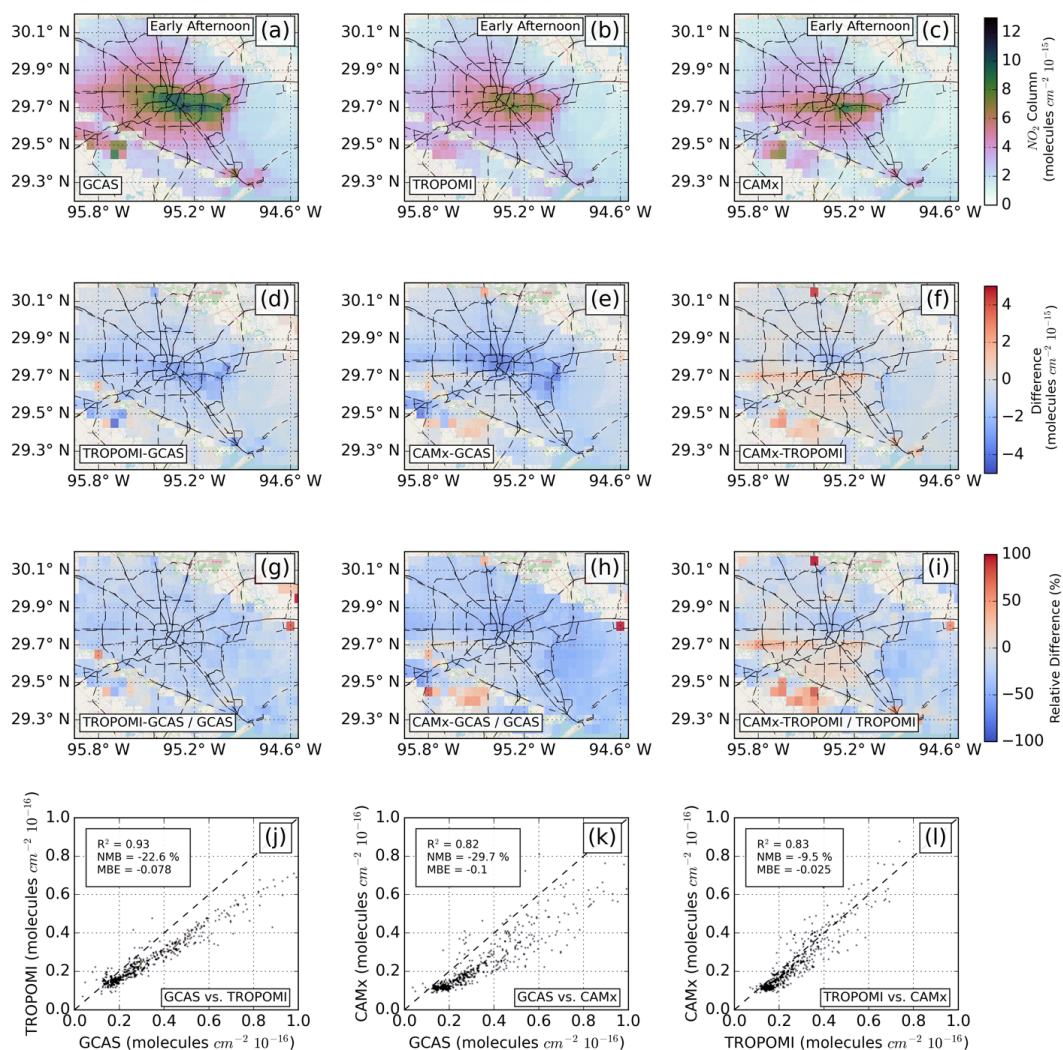


460 molecules $\text{cm}^{-2} 10^{15}$ (Figure 5E). Visually, the negative bias in CAMx appears to be stronger in downtown and to the west, east, and north-west of downtown and less to the south and south-west of downtown. Overall, GCAS and CAMx are well correlated ($r^2=0.74$) (Figure 5K); however, simulated columns from CAMx have a worse negative bias (NMB=-31.0%) against GCAS than what is captured at the Pandora sites of approximately -26%. Around some point sources CAMx columns are positively biased against GCAS observations. This high bias in CAMx is likely attributable to differences in wind speed and direction in the WRF simulation than in reality. These differences could contribute to NO_2 plumes being advected in incorrect directions.

465 Lastly, when comparing observed columns from TROPOMI to simulated columns from CAMx, biases have a great degree of spatial variability; however, in general CAMx is negatively biased. In a relative sense (Fig. 5I), the CAMx simulated columns are lowest compared to TROPOMI in the rural bay (-26%) and similar in downtown (-11%) and in the background (-7%). There are a few areas where this pattern does not hold: both in the area southwest of downtown Houston and near point sources, CAMx is biased high compared to TROPOMI. These results indicate
470 that simulated columns from CAMx are underestimated in downtown Houston and that this underestimation could potentially be attributable to an incorrect advection of NO_2 from some downtown source to the south-west perhaps in conjunction with an underestimate of emissions in this downtown area. Overall, TROPOMI and CAMx are well correlated ($r^2=0.73$) and there is a spatially heterogeneous low bias when considering the two products throughout the domain (NMB = -9.7%) (Fig. 5L).

475 3.4 Comparisons of GCAS, TROPOMI, and CAMx data at a coarser resolution

The comparisons presented in the prior section are done at the high resolution of the CAMx grid ($444 \times 444 \text{ m}^2$). Here, we characterize the effect of the coarser resolution of TROPOMI by performing an additional comparison of the three datasets at the $0.05^\circ \times 0.05^\circ$ resolution (approximately $5.5 \times 5.5 \text{ km}^2$) (Fig. 6). We average all of the NO_2
480 columns from this finer resolution to the coarser resolution based on the centroid of the fine resolution grid cells. This new coarser resolution is comparable to that of the TROPOMI observations at nadir (on average $3.5 \times 5.5 \text{ km}^2$). We additionally present comparisons at two further coarser resolutions in the supplemental: $0.25^\circ \times 0.25^\circ$ (Fig. S13) and $0.1^\circ \times 0.1^\circ$ (Fig. S14).



485

Figure 6: Spatial distribution of GCAS (A), TROPOMI (B), and CAMx (C) at the $0.05^\circ \times 0.05^\circ$ resolution averaged across the ten GCAS flight days when within 1.5 hours of each TROPOMI overpass representing early afternoon NO₂ columns. Absolute differences between GCAS and TROPOMI (D), GCAS and CAMx (E), and TROPOMI and CAMx (F). Relative differences between GCAS and TROPOMI (G), GCAS and CAMx (E), and TROPOMI and CAMx (F). Scatter density plots of GCAS vs. TROPOMI (G), GCAS vs.

490



CAMx (H), and TROPOMI vs. CAMx (I). © OpenStreetMap contributors 2023. Distributed under the Open Data Commons Open Database License (ODbL) v1.0.

495 Generally, this change in resolution has only a minor effect on the trends discussed in the prior section. Observed
NO₂ columns from GCAS and TROPOMI have a collocated peak in downtown Houston and NO₂ columns from
TROPOMI are still systematically biased lower compared to GCAS. Simulated NO₂ columns from CAMx are
clearly lower than GCAS in the area directly west of downtown and slightly higher southwest of downtown
compared to TROPOMI (Fig. 6A-C). Considering the spatial distribution of absolute (Fig. 6D-F) and relative (Fig.
6G-I) differences between the three products, the low bias in TROPOMI compared to GCAS is generally
500 homogenous throughout the domain. On the other hand, there are clear peaks in negative biases in downtown and
western Houston when comparing CAMx to GCAS and in some areas southwest of downtown biases are small and
positive. Averaging observations to this coarser resolution improved the correlation for all three pairs ($r^2=0.93$, 0.82 ,
and 0.83 for GCAS and TROPOMI, GCAS and CAMx, and TROPOMI and CAMx, respectively) while the biases
remained comparable to what was found in the comparison at a finer resolution (Fig. 5J-L).

505 **3.5 Weekend vs. weekday patterns across the datasets**

Three of the ten GCAS flight days occurred on weekends (September 11th, 25th, and 26th) and observations from
GCAS and TROPOMI – along with simulated NO₂ columns from CAMx – exhibited different patterns on weekends
versus on weekdays (September 1st, 3rd, 8-10th, 23rd, 24th). This difference in observed and simulated patterns is
explored in greater detail in this section, first through comparisons to Pandora measurements (Fig. 7) and then
510 through spatial comparisons of the products on weekdays versus on weekends (Fig. 8). When interpreting these
results, it should be considered that weekend data is limited to only three days. This data sparsity introduces a high
degree of uncertainty in conclusions derived from this analysis. Day to day changes in meteorological conditions are
likely responsible for some of the exhibited differences so they cannot solely be attributed to differences in emission
patterns.



515

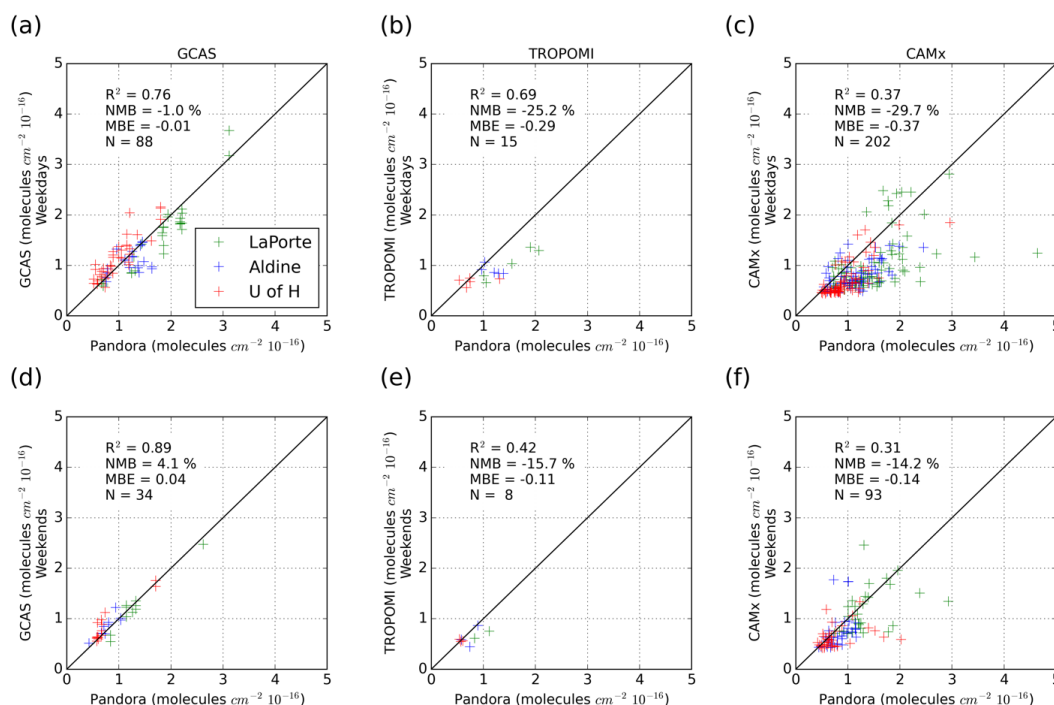


Figure 7: Comparison of GCAS (A), TROPOMI (B), and CAMx (C) to Pandora on weekdays and of GCAS (D), TROPOMI (E), and CAMx (F) to Pandora on weekends. Data from all possible overpasses coincident within 15 minutes of a Pandora observation are considered. GCAS flight times generally ranged from 8:00 AM-4:00 PM CDT. TROPOMI overpasses occurred around 1:30 PM local time.

520

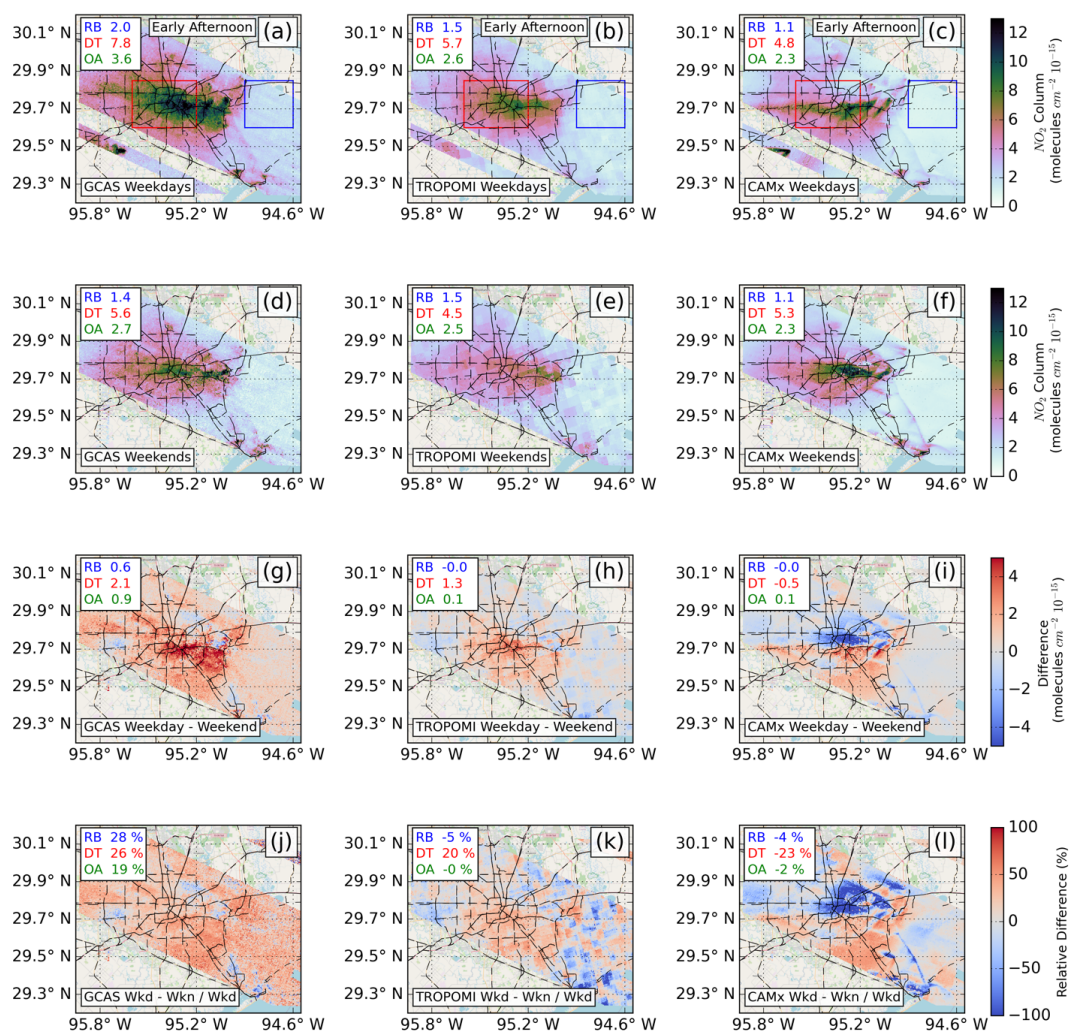
First, we consider how comparisons of the observational datasets – GCAS and TROPOMI – with Pandora change on weekends compared to weekdays. Biases for both GCAS and TROPOMI become more positive on weekends, NMB=4.1% and NMB=-15.7%, respectively, than on weekdays, NMB=-1.0% and NMB=-25.2%. GCAS observations are slightly better correlated to Pandora measurements on weekends ($r^2=0.89$ versus $r^2=0.76$); however, TROPOMI observations are worse correlated ($r^2=0.42$ versus $r^2=0.69$) that is likely attributable to a limited number of observations that are at lower NO₂ column levels with limited dynamic range. Overall, biases are slightly worse for GCAS and better for TROPOMI on weekends; however, given the small number of measurements it is unclear whether this pattern is attributable to meteorological conditions or if it is attributable to some systematic bias in the instruments.

530

Simulated NO₂ columns from CAMx exhibit clearer weekday versus weekend patterns, and since these simulated columns are available for every hour of the day there is a greater number of measurements to support these findings



535 than for the two observational datasets. While the correlation is slightly degraded on weekends ($r^2=0.31$ versus $r^2=0.37$) the negative bias in simulated columns compared to Pandora measurements is reduced on weekends (NMB=-29.7% versus NMB=-14.2%).



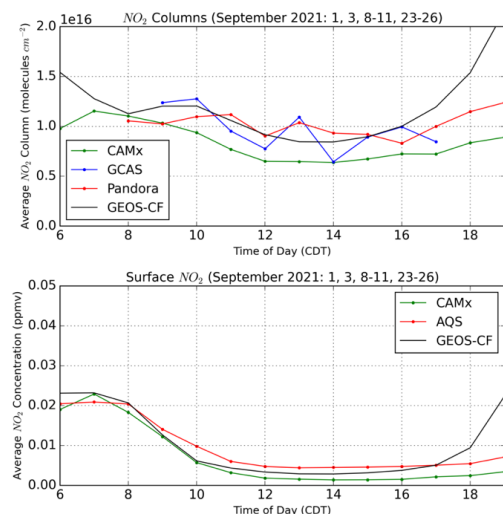
540 **Figure 8: Spatial Distribution of GCAS, TROPOMI, and CAMx NO₂ columns on weekdays (A-C), weekends (D-F), and the absolute difference between weekdays and weekends (G-I) and relative difference (J-L). Data are averaged across the GCAS flight days corresponding to weekdays or weekends when within 1.5 hours of each TROPOMI overpass representing early afternoon NO₂ columns. We identify three distinct areas: downtown or “DT” (red), the low emissions East Galveston Bay or “RB” (blue), and all other areas or “OA” (green) and calculate the averages in the top left of each chart. © OpenStreetMap contributors 2023.**
 545 **Distributed under the Open Data Commons Open Database License (ODbL) v1.0.**



GCAS and TROPOMI observations of NO_2 column concentrations are higher on weekdays (Fig. 8A, B) than on weekends (Fig. 8D, E). This is true in downtown Houston and the rural bay where weekday GCAS observations are
550 2.1 molecules $\text{cm}^{-2} 10^{15}$ (26%) and 0.6 molecules $\text{cm}^{-2} 10^{15}$ (28%) higher, respectively, on weekdays than on weekends. In other areas of Houston, GCAS observations on weekdays are higher than weekends but not to the same degree (19%). A similar pattern occurs for TROPOMI, in downtown Houston TROPOMI columns are 20% higher on weekdays than on weekends but comparable in other areas and -5% lower in the rural bay. This comparison again implicates some underestimated weekday source of NO_2 in CAMx that is of great importance in
555 the western area of Houston; however, due to the lack of data on weekends – that is apparent in the discontinuities in the weekend NO_2 column concentrations of TROPOMI – it is difficult to examine this quantitatively.

Comparing weekday columns simulated from CAMx with weekend columns, we find that the mean concentrations for the three defined areas are nearly identical (Fig. 8C and F), although columns on weekdays are higher south and southwest of downtown while columns on weekends are higher within downtown. These spatial patterns are further revealed in the difference plots (Fig. 8I and 8L) where the difference in weekday versus weekend values appear to be split right along I-10; north of I-10 weekday values are much lower than weekend values while south of I-10 the opposite is true. This difference is likely attributable to different meteorological conditions on these days. Overall, simulated CAMx columns are substantially lower than GCAS and TROPOMI on weekdays but more similar on
565 weekends implying that weekday emissions may be underestimated in the TCEQ inventory.

3.6 Diurnal patterns in column and surface NO_2





570 **Figure 9: Diurnal patterns in NO₂ columns (top) averaged across the three Pandora sites and 10 flight days from CAMx (green), GCAS (blue), Pandora (red), and GEOS-CF (black). Diurnal patterns in surface-level NO₂ concentrations (bottom) in downtown Houston for CAMx and GEOS-CF averaged across the 10 flight days and across all monitors in Harris County for AQS surface-level monitors (red).**

575 Lastly, we characterize the diurnal profiles of simulated and observed NO₂ columns during the TRACER-AQ campaign in downtown Houston (Fig. 9). First, considering column concentrations, we find generally good agreement during the late morning (8 am-10 am) across the two simulated datasets (CAMx and GEOS-CF) and two observational datasets (GCAS and Pandora). During midday and the afternoon (11 am-4 pm) – that corresponds to the period with the most GCAS observations – GEOS-CF columns generally agree well with Pandora observations. In the evening (5pm-7pm), GEOS-CF columns have a substantial high bias across these flight days. While CAMx is
580 low biased throughout most of the day it maintains the same magnitude of change as Pandora reflecting a similar temporal pattern. Second, considering surface concentrations, we see a similar trend. Generally, there is great agreement across the three datasets (CAMx, AQS observations, and GEOS-CF) in the morning (6 am-9 am) before they begin to diverge with the two simulated products maintaining comparable magnitudes with low biases compared to surface monitors. At around midday to the afternoon (12 pm-5 pm) both simulated products have a low
585 bias compared to observed surface-level NO₂; however, the bias in CAMx concentrations is worse. Some of the apparent low bias may be related to an artificial high bias in NO₂ chemiluminescence surface monitors (Dunlea et al., 2007; Lamsal et al., 2008). In the evening (6 pm-7 pm), surface-level NO₂ from GEOS-CF climbs rapidly; however, observed NO₂ from the AQS and simulated NO₂ from CAMx stably increase only slightly. This large increase in NO₂ in the evening appears at both the surface and in the column in GEOS-CF indicating a consistent
590 high bias as the boundary layer height decreases which is perhaps attributable to its coarser horizontal and vertical resolution. Overall, simulated surface concentrations and column concentrations from CAMx appear to perform at their worst during the late morning and afternoon compared to observations from Pandora, GCAS, and AQS monitors and there is greater agreement in the early morning and evening.

4 Conclusions

595 This study leveraged observational datasets of NO₂ column densities from three instruments – Pandora ground-based spectrometers, the airborne GCAS instrument, and the satellite TROPOMI instrument. These instruments were used to investigate NO₂ column densities in Houston, TX during the September 2021 TRACER-AQ campaign and to characterize strengths/weaknesses and uncertainties in the respective datasets. These observational datasets were then compared to simulated NO₂ columns from CAMx to characterize the performance of the simulation and to
600 identify potential under- or overestimates of emissions in the simulation. We find that GCAS has strong agreement with Pandora instruments ($r^2=0.80$ and $NMB=0.1\%$) during its overpasses and that TROPOMI also has strong performance but an important low bias – consistent with validation by the European Space Agency (Verhoelst et al., 2021) – across the urban Houston locations ($r^2=0.73$ and $NMB=-22.8\%$). This low bias in TROPOMI observations



605 persists despite the inclusion of an air mass factor derived from the CAMx simulation. When comparing different
versions of TROPOMI we find differences between the v2.3.1, v2.4.0, and NASA MINDS product and find that the
MINDS ($r^2=0.69$ and $NMB=-18.2\%$) and version 2.3.1 ($r^2=0.72$ and $NMB=-18.3\%$) products – with the CAMx
AMF – performs comparably but both outperform version 2.4.0. The performance of the CAMx simulation varied
depending on the day, but overall, simulated NO_2 columns were more poorly correlated and more negatively biased
610 bias in CAMx simulated NO_2 columns improved on weekends ($NMB=-14.2\%$) – albeit over a limited number of
days. This improvement on weekends implicates that a source that emits in greater amounts on weekdays (e.g.,
heavy-duty vehicles) could be underestimated in the TCEQ inventory; however, we cannot say this conclusively
given the limited number of observations on weekends. The poor correlation in the simulated NO_2 columns is likely
attributable to minor wind directional errors and spatial correlations over larger extents match well.

615

When we compare the spatial distribution of TROPOMI observations to GCAS (Fig. 3 and 4) we find that the low
bias in TROPOMI NO_2 columns is perhaps stronger than the low bias implied at the three Pandora sites – this could
be a resolution constraint of the coarser TROPOMI product that is unable to capture the fine-scale features in NO_2
column concentrations that GCAS is able to. If coarse resolution is responsible for this low-bias, new instruments on
620 geostationary satellites from missions like the NASA Tropospheric Emissions: Monitoring of Pollution (TEMPO)
mission could be leveraged to further improve satellite-derived estimates of urban NO_2 in cities like Houston.
CAMx comparisons to GCAS, when extended beyond the limited number of Pandora sites, indicate that the CAMx
simulated low bias could be substantially worse (-31.0%) in downtown and west of downtown Houston. This overall
underestimate in the CAMx simulations is potentially attributable to a number of confounding factors including an
625 inability of the WRF simulation to capture local meteorology and an underestimate of emissions in sectors that are
more spatially located in downtown and western Houston like on-road mobile emissions. We also consider
differences in the diurnal profiles of surface and column NO_2 across multiple datasets and find that the performance
of CAMx is at its worst in the late morning and early afternoon and performance is better during other times of the
day.

630

There is a clear negative bias in the CAMx simulated NO_2 columns compared to observations. Additionally, the low
bias in the TROPOMI observations compared to Pandora and GCAS merits further investigation; the role of algorithm
and resolution could be considered by comparing different versions and finer-resolution geostationary observations in
the future beyond what is considered in this study. The reference background NO_2 from TROPOMI used in GCAS
635 could also introduce error into these results that should be considered. Given the fine resolution of GCAS observations
and CAMx simulated column concentrations there is potential for investigations into how air pollution is inequitably
distributed across different populations in Houston and how specific sources contribute to these inequities. The
findings presented here imply that TROPOMI derived NO_2 column concentrations may be underestimated in Houston
if not corrected for in applications such as exposure assessments, and NO_x emissions derivations. This analysis
640 benefitted from three independent measurement datasets (i.e., Pandora, TROPOMI, and GCAS) that were critical to



isolate the negative biases in TROPOMI and CAMx. It is common to consider TROPOMI measurements as accurate representation of NO₂ column concentrations; however, if we had done so in this study, we would have failed to identify the substantial negative bias in the CAMx simulation of column concentrations. Observations from multiple Pandora instruments and GCAS overpasses made it possible to isolate negative biases in TROPOMI and CAMx.
645 Lastly, biases in simulated CAMx column concentrations imply that current TCEQ emissions inventories used to drive the CAMx simulation may be underestimated, and that this underestimation is likely attributable to a source with substantial weekday-weekend differences and correlated with roadways and/or population density.

Acknowledgements

The authors of this paper acknowledge Elena Lind, Alex Kotsakis, the NASA Pandora Project and LuftBlick for their contribution in deploying, operating, and processing data from the Pandora spectrometers during TRACER-AQ, the
650 NASA Tropospheric Composition Program and the Texas Commission on Environmental Quality for TRACER-AQ support, and the TRACER-AQ science team for their useful contributions. We also acknowledge the use of Google Earth for the background map used in Fig. 1. The authors acknowledge the use of OpenStreetMaps for the background maps in Fig. 2, 4, 5, 6, 8 and S2-14. The authors also acknowledge funding from the NASA Atmospheric Composition
655 Modelling and Analysis Program (ACMAP) (80NSSC23K1002). The preparation of this manuscript was funded by a grant from the Texas Air Quality Research Program (AQRP) at The University of Texas at Austin through the Texas Emission Reduction Program (TERP) and the Texas Commission on Environmental Quality (TCEQ). The findings, opinions and conclusions are the work of the authors and do not necessarily represent findings, opinions, or conclusions of the AQRP or the TCEQ.

660 Code Availability

The scripts used to process these data for the intercomparison are available by correspondence with the authors upon reasonable request.

Data Availability

Ground level EPA AQS observations are available from EPA Air Data: [https://www.epa.gov/outdoor-air-quality-](https://www.epa.gov/outdoor-air-quality-data)
665 [data](https://www.epa.gov/outdoor-air-quality-data). GEOS-CF data are available from the GrADS data server: <https://opendap.nccs.nasa.gov/dods/>. TROPOMI NO₂ column data are publicly available from the Copernicus Data Space Ecosystem: <https://dataspace.copernicus.eu>. GCAS and CAMx data are publicly available via NASA's Atmospheric Sciences Data Center: https://doi.org/10.5067/ASDC/SUBORBITAL/TRACERAQ/DATA001/GV/AircraftRemoteSensing/GCAS_1 as
670 are Pandora data https://asdc.larc.nasa.gov/project/TRACER-AQ/TRACERAQ_Pandora_Data_1.



Author Contributions

D.G., developed the project design, J.J. and G.Y. set-up and conducted the WRF-CAMx simulations, L.J. and the TRACER-AQ science team measured and processed the GCAS and Pandora Data, D.G. downloaded and processed the TROPOMI Data and regridded all data to the WRF-CAMx grid, M.O.N. further processed the data to match
675 temporally and spatially, conducted the intercomparison, wrote the manuscript, and generated the figures except Fig. 1 and Fig. S14 that were generated by J.J. and D.G., respectively, B.D. gave feedback on the methodology, all authors edited the manuscript and gave feedback on the figures.

Competing Interests

The authors declare that they have no conflict of interest.

680 References

- Achakulwisut, P., Brauer, M., Hystad, P., & Anenberg, S. C. (2019). Global, national, and urban burdens of paediatric asthma incidence attributable to ambient NO₂ pollution: Estimates from global datasets. *The Lancet Planetary Health*, 3(4), e166–e178. [https://doi.org/10.1016/S2542-5196\(19\)30046-4](https://doi.org/10.1016/S2542-5196(19)30046-4)
- Anenberg, S. C., Mohegh, A., Goldberg, D. L., Kerr, G. H., Brauer, M., Burkart, K., Hystad, P., Larkin, A., Wozniak,
685 S., & Lamsal, L. (2022). Long-term trends in urban NO₂ concentrations and associated paediatric asthma incidence: Estimates from global datasets. *The Lancet Planetary Health*, 6(1), e49–e58. [https://doi.org/10.1016/S2542-5196\(21\)00255-2](https://doi.org/10.1016/S2542-5196(21)00255-2)
- Bucsela, E. J., Krotkov, N. A., Celarier, E. A., Lamsal, L. N., Swartz, W. H., Bhartia, P. K., Boersma, K. F., Veefkind, J. P., Gleason, J. F., & Pickering, K. E. (2013). A new stratospheric and tropospheric NO₂
690 retrieval algorithm for nadir-viewing satellite instruments: Applications to OMI. *Atmospheric Measurement Techniques*, 6(10), 2607–2626. <https://doi.org/10.5194/amt-6-2607-2013>
- Cede, A. (2021). *Manual for Blick Software Suite 1.8*.
- Danckaert, T., Fayt, C., Roozendaal, M. V., Smedt, I. D., Letocart, V., Merlaud, A., & Pinardi, G. (2017). *QDOAS Software user manual*.
- 695 de Foy, B., Lei, W., Zavala, M., Volkamer, R., Samuelsson, J., Mellqvist, J., Galle, B., Martínez, A.-P., Grutter, M., Retama, A., & Molina, L. T. (2007). Modelling constraints on the emission inventory and on vertical



- dispersion for CO and SO₂ in the Mexico City Metropolitan Area using Solar FTIR and zenith sky UV spectroscopy. *Atmospheric Chemistry and Physics*, 7(3), 781–801. <https://doi.org/10.5194/acp-7-781-2007>
- 700 de Foy, B., Wilkins, J. L., Lu, Z., Streets, D. G., & Duncan, B. N. (2014). Model evaluation of methods for estimating surface emissions and chemical lifetimes from satellite data. *Atmospheric Environment*, 98, 66–77. <https://doi.org/10.1016/j.atmosenv.2014.08.051>
- Demetillo, M. A. G., Navarro, A., Knowles, K. K., Fields, K. P., Geddes, J. A., Nowlan, C. R., Janz, S. J., Judd, L. M., Al-Saadi, J., Sun, K., McDonald, B. C., Diskin, G. S., & Pusede, S. E. (2020). Observing Nitrogen Dioxide Air Pollution Inequality Using High-Spatial-Resolution Remote Sensing Measurements in
- 705 Houston, Texas. *Environmental Science & Technology*, 54(16), 9882–9895. <https://doi.org/10.1021/acs.est.0c01864>
- DOC/NOAA/NWS/NCEP/EMC. (2023). *Global Data Assimilation System (GDAS)* [dataset]. <https://www.ncei.noaa.gov/access/metadata/landing-page>.
- Dunlea, E. J., Herndon, S. C., Nelson, D. D., Volkamer, R. M., Martini, F. S., Sheehy, P. M., Zahniser, M. S.,
- 710 Shorter, J. H., Wormhoudt, J. C., Lamb, B. K., Allwine, E. J., Gaffney, J. S., Marley, N. A., Grutter, M., Marquez, C., Blanco, S., Cardenas, B., Retama, A., Villegas, C. R. R., ... Molina, M. J. (2007). Evaluation of nitrogen dioxide chemiluminescence monitors in a polluted urban environment. *Atmos. Chem. Phys.*, 14.
- EPA. (2023). *United States Environmental Protection Agency (EPA). "Clean Air Markets Program Data."* Washington, DC: Office of Atmospheric Protection, Clean Air Markets Division. Available from EPA's Air
- 715 Markets Program Data web site: <https://campd.epa.gov/>. [dataset]. <https://campd.epa.gov/>.
- Eskes, H. J., Eichmann, K.-U., Lambert, J.-C., Loyola, D., Stein-Zweers, D., Dehn, A., & Zehner, C. (2023). *S5P MPC Product Readme Nitrogen Dioxide*.
- European Space Agency. (2021). *Copernicus Sentinel-5P TROPOMI* [dataset]. European Space Agency. <https://doi.org/10.5270/S5P-9bnp8q8>
- 720 Ge, S., Wang, S., Xu, Q., & Ho, T. (2021). Source apportionment simulations of ground-level ozone in Southeast Texas employing OSAT/APCA in CAMx. *Atmospheric Environment*, 253, 118370. <https://doi.org/10.1016/j.atmosenv.2021.118370>



- Goldberg, D. L., Harkey, M., de Foy, B., Judd, L., Johnson, J., Yarwood, G., & Holloway, T. (2022). Evaluating NO_x emissions and their effect on O₃ production in Texas using TROPOMI NO₂ and HCHO. *Atmospheric Chemistry and Physics*, 22(16), 10875–10900. <https://doi.org/10.5194/acp-22-10875-2022>
- 725
- Guenther, A. B., Jiang, X., Heald, C. L., Sakulyanontvittaya, T., Duhl, T., Emmons, L. K., & Wang, X. (2012). The Model of Emissions of Gases and Aerosols from Nature version 2.1 (MEGAN2.1): An extended and updated framework for modeling biogenic emissions. *Geoscientific Model Development*, 5(6), 1471–1492. <https://doi.org/10.5194/gmd-5-1471-2012>
- 730
- Herman, J., Cede, A., Spinei, E., Mount, G., Tzortziou, M., & Abuhassan, N. (2009). NO₂ column amounts from ground-based Pandora and MFDOAS spectrometers using the direct-sun DOAS technique: Intercomparisons and application to OMI validation. *Journal of Geophysical Research: Atmospheres*, 114(D13). <https://doi.org/10.1029/2009JD011848>
- Huang, S., Li, H., Wang, M., Qian, Y., Steenland, K., Caudle, W. M., Liu, Y., Sarnat, J., Papatheodorou, S., & Shi, L. (2021). Long-term exposure to nitrogen dioxide and mortality: A systematic review and meta-analysis. *The Science of the Total Environment*, 776, 145968. <https://doi.org/10.1016/j.scitotenv.2021.145968>
- 735
- Hudman, R. C., Moore, N. E., Mebust, A. K., Martin, R. V., Russell, A. R., Valin, L. C., & Cohen, R. C. (2012). Steps towards a mechanistic model of global soil nitric oxide emissions: Implementation and space based-constraints. *Atmospheric Chemistry and Physics*, 12(16), 7779–7795. <https://doi.org/10.5194/acp-12-7779-2012>
- 740
- Jaeglé, L., Jacob, D., Wang, Y., Weinheimer, A., Ridley, B., Campos, T., Sachse, G., & Hagen, D. (1998). Sources and chemistry of NO_x in the upper troposphere over the United States. *Geophysical Research Letters - GEOPHYS RES LETT*, 25, 1705–1708. <https://doi.org/10.1029/97GL03591>
- Jia, J., Cheng, S., Liu, L., Lang, J., Wang, G., Chen, G., & Liu, X. (2017). An Integrated WRF-CAMx Modeling Approach for Impact Analysis of Implementing the Emergency PM_{2.5} Control Measures during Red Alerts in Beijing in December 2015. *Aerosol and Air Quality Research*, 17(10), 2491–2508. <https://doi.org/10.4209/aaqr.2017.01.0009>
- 745
- Jin, X., Zhu, Q., & Cohen, R. C. (2021). Direct estimates of biomass burning NO_x emissions and lifetimes using daily observations from TROPOMI. *Atmospheric Chemistry and Physics*, 21(20), 15569–15587. <https://doi.org/10.5194/acp-21-15569-2021>
- 750



- Judd, L. M., Al-Saadi, J. A., Szykman, J. J., Valin, L. C., Janz, S. J., Kowalewski, M. G., Eskes, H. J., Veeffkind, J. P., Cede, A., Mueller, M., Gebetsberger, M., Swap, R., Pierce, R. B., Nowlan, C. R., Abad, G. G., Nehrir, A., & Williams, D. (2020). Evaluating Sentinel-5P TROPOMI tropospheric NO₂ column densities with airborne and Pandora spectrometers near New York City and Long Island Sound. *Atmospheric Measurement Techniques*, 13(11), 6113–6140. <https://doi.org/10.5194/amt-13-6113-2020>
- 755
- Keller, C. A., Knowland, K. E., Duncan, B. N., Liu, J., Anderson, D. C., Das, S., Lucchesi, R. A., Lundgren, E. W., Nicely, J. M., Nielsen, E., Ott, L. E., Saunders, E., Strode, S. A., Wales, P. A., Jacob, D. J., & Pawson, S. (2021). Description of the NASA GEOS Composition Forecast Modeling System GEOS-CF v1.0. *Journal of Advances in Modeling Earth Systems*, 13(4), e2020MS002413. <https://doi.org/10.1029/2020MS002413>
- 760
- Kim, S.-W., McKeen, S. A., Frost, G. J., Lee, S.-H., Trainer, M., Richter, A., Angevine, W. M., Atlas, E., Bianco, L., Boersma, K. F., Brioude, J., Burrows, J. P., de Gouw, J., Fried, A., Gleason, J., Hilboll, A., Mellqvist, J., Peischl, J., Richter, D., ... Williams, E. (2011). Evaluations of NO_x and highly reactive VOC emission inventories in Texas and their implications for ozone plume simulations during the Texas Air Quality Study 2006. *Atmospheric Chemistry and Physics*, 11(22), 11361–11386. [https://doi.org/10.5194/acp-11-11361-](https://doi.org/10.5194/acp-11-11361-2011)
- 765
- 2011
- Kowalewski, M. G., & Janz, S. J. (2014). Remote sensing capabilities of the GeoCAPE Airborne Simulator. *Earth Observing Systems XIX, 9218*, 496–507. <https://doi.org/10.1117/12.2062058>
- Lambert, J.-C., Claas, J., Stein-Zweers, D., Ludewig, A., Loyola, D., Sneep, M., & Dehn, A. (2023). *Quarterly Validation Report of the Copernicus Sentinel-5 Precursor Operational Data Products #19*.
- 770
- Lamsal, L. N., Krotkov, N. A., Marchenko, S. V., Joiner, J., Oman, L., Vasilkov, A., Fisher, B., Qin, W., Yang, E.-S., Fasnacht, Z., Choi, S., Leonard, P., & Haffner, D. (2022). *TROPOMI/S5P NO₂ Tropospheric, Stratospheric and Total Columns MINDS 1-Orbit L2 Swath 5.5 km x 3.5 km, NASA Goddard Space Flight Center, Goddard Earth Sciences Data and Information Services Center*.
- Lamsal, L. N., Martin, R. V., van Donkelaar, A., Steinbacher, M., Celarier, E. A., Bucsela, E., Dunlea, E. J., & Pinto, J. P. (2008). Ground-level nitrogen dioxide concentrations inferred from the satellite-borne Ozone Monitoring Instrument. *Journal of Geophysical Research: Atmospheres*, 113(D16). <https://doi.org/10.1029/2007JD009235>
- 775



- Leitch, J. W., Delker, T., Good, W., Ruppert, L., Murcay, F., Chance, K., Liu, X., Nowlan, C., Janz, S. J., Krotkov, N. A., Pickering, K. E., Kowalewski, M., & Wang, J. (2014). The GeoTASO airborne spectrometer project. *Earth Observing Systems XIX, 9218*, 487–495. <https://doi.org/10.1117/12.2063763>
- 780
- Li, W., Wang, Y., Liu, X., Soleimanian, E., Griggs, T., Flynn, J., & Walter, P. (2023). Understanding offshore high-ozone events during TRACER-AQ 2021 in Houston: Insights from WRF-CAMx photochemical modeling. *EGUsphere*, 1–21. <https://doi.org/10.5194/egusphere-2023-1117>
- Lorente, A., Boersma, K. F., Eskes, H. J., Veeffkind, J. P., van Geffen, J. H. G. M., de Zeeuw, M. B., Denier van der Gon, H. a. C., Beirle, S., & Krol, M. C. (2019). Quantification of nitrogen oxides emissions from build-up of pollution over Paris with TROPOMI. *Scientific Reports, 9*(1), Article 1. <https://doi.org/10.1038/s41598-019-56428-5>
- 785
- Luke, W. T., Kelley, P., Lefer, B. L., Flynn, J., Rappenglück, B., Leuchner, M., Dibb, J. E., Ziemba, L. D., Anderson, C. H., & Buhr, M. (2010). Measurements of primary trace gases and NO_y composition in Houston, Texas. *Atmospheric Environment, 44*(33), 4068–4080. <https://doi.org/10.1016/j.atmosenv.2009.08.014>
- 790
- Mazzuca, G. M., Ren, X., Loughner, C. P., Estes, M., Crawford, J. H., Pickering, K. E., Weinheimer, A. J., & Dickerson, R. R. (2016). Ozone production and its sensitivity to NO_x and VOCs: Results from the DISCOVER-AQ field experiment, Houston 2013. *Atmospheric Chemistry and Physics, 16*(22), 14463–14474. <https://doi.org/10.5194/acp-16-14463-2016>
- 795
- McDuffie, E. E., Smith, S. J., O'Rourke, P., Tibrewal, K., Venkataraman, C., Marais, E. A., Zheng, B., Crippa, M., Brauer, M., & Martin, R. V. (2020). A global anthropogenic emission inventory of atmospheric pollutants from sector- and fuel-specific sources (1970–2017): An application of the Community Emissions Data System (CEDS). *Earth System Science Data, 12*(4), 3413–3442. <https://doi.org/10.5194/essd-12-3413-2020>
- Miller, D. J., Actkinson, B., Padilla, L., Griffin, R. J., Moore, K., Lewis, P. G. T., Gardner-Frolick, R., Craft, E., Portier, C. J., Hamburg, S. P., & Alvarez, R. A. (2020). Characterizing Elevated Urban Air Pollutant Spatial Patterns with Mobile Monitoring in Houston, Texas. *Environmental Science & Technology, 54*(4), 2133–2142. <https://doi.org/10.1021/acs.est.9b05523>
- 800
- Murray, L. T. (2016). Lightning NO_x and Impacts on Air Quality. *Current Pollution Reports, 2*(2), 115–133. <https://doi.org/10.1007/s40726-016-0031-7>
- 805
- NASA. (2023). *EOSDIS Worldview*. <https://worldview.earthdata.nasa.gov/>



- NASA/LARC/SD/ASDC. (2022). *TRACER-AQ JSC G-V Aircraft Remotely Sensed GEOstationary Coastal and Air Pollution Events (GEO-CAPE) Airborne Simulator (GCAS) Data*. NASA Langley Atmospheric Science Data Center DAAC.
<https://doi.org/10.5067/ASDC/SUBORBITAL/TRACERAQ/DATA001/GV/AircraftRemoteSensing/GCAS>
- 810 _1
- Nowlan, C. R., Liu, X., Janz, S. J., Kowalewski, M. G., Chance, K., Follette-Cook, M. B., Fried, A., González Abad, G., Herman, J. R., Judd, L. M., Kwon, H.-A., Loughner, C. P., Pickering, K. E., Richter, D., Spinei, E., Walega, J., Weibring, P., & Weinheimer, A. J. (2018). Nitrogen dioxide and formaldehyde measurements from the GEOstationary Coastal and Air Pollution Events (GEO-CAPE) Airborne Simulator over Houston, Texas. *Atmospheric Measurement Techniques*, *11*(11), 5941–5964. <https://doi.org/10.5194/amt-11-5941-2018>
- 815
- Palmer, P. I., Jacob, D. J., Chance, K., Martin, R. V., Spurr, R. J. D., Kurosu, T. P., Bey, I., Yantosca, R., Fiore, A., & Li, Q. (2001). Air mass factor formulation for spectroscopic measurements from satellites: Application to formaldehyde retrievals from the Global Ozone Monitoring Experiment. *Journal of Geophysical Research: Atmospheres*, *106*(D13), 14539–14550. <https://doi.org/10.1029/2000JD900772>
- 820
- Ramboll. (2022a). Enhance MARINER Tool for Commercial Marine Emission Inventories Final Report. *Final Report*.
- Ramboll. (2022b). *User's Guide COMPREHENSIVE AIR QUALITY MODEL WITH EXTENSIONS Version 7.20*.
https://camx-wp.azurewebsites.net/Files/CAMxUsersGuide_v7.20.pdf
- 825
- Riess, T. C. V. W., Boersma, K. F., Van Roy, W., de Laat, J., Dammers, E., & van Vliet, J. (2023). To new heights by flying low: Comparison of aircraft vertical NO₂ profiles to model simulations and implications for TROPOMI NO₂ retrievals. *Atmospheric Measurement Techniques*, *16*(21), 5287–5304.
<https://doi.org/10.5194/amt-16-5287-2023>
- Soleimanian, E., Wang, Y., Li, W., Liu, X., Griggs, T., Flynn, J., Walter, P. J., & Estes, M. J. (2023). Understanding ozone episodes during the TRACER-AQ campaign in Houston, Texas: The role of transport and ozone production sensitivity to precursors. *Science of The Total Environment*, *900*, 165881.
<https://doi.org/10.1016/j.scitotenv.2023.165881>
- 830



- TCEQ. (2021). *SIP Revision: Regional Haze*. Texas Commission on Environmental Quality.
https://www.tceq.texas.gov/airquality/sip/bart/haze_sip.html
- 835 United States Census Bureau. (2022, June 13). *Metropolitan and Micropolitan Statistical Areas Population Totals: 2020-2022*. Census.Gov. <https://www.census.gov/data/tables/time-series/demo/popest/2020s-total-metro-and-micro-statistical-areas.html>
- van Geffen, J., Eskes, H., Compernolle, S., Pinardi, G., Verhoelst, T., Lambert, J.-C., Sneep, M., ter Linden, M., Ludewig, A., Boersma, K. F., & Veeffkind, J. P. (2022). Sentinel-5P TROPOMI NO₂ retrieval: Impact of version v2.2 improvements and comparisons with OMI and ground-based data. *Atmospheric Measurement Techniques*, 15(7), 2037–2060. <https://doi.org/10.5194/amt-15-2037-2022>
- 840 van Geffen, J., Eskes, H. J., Compernolle, S., Pinardi, G., Verhoelst, T., & Lambert, J.-C. (2021). Sentinel-5P TROPOMI NO₂ retrieval: Impact of version v2.2 improvements and comparisons with OMI and ground-based data. *Atmospheric Measurement Techniques*, 15(7), 2037–2060. <https://doi.org/10.5194/AMT-15-2037-2022>
- 845 Verhoelst, T., Compernolle, S., Pinardi, G., Lambert, J.-C., Eskes, H. J., Eichmann, K.-U., Fjæraa, A. M., Granville, J., Niemeijer, S., Cede, A., Tiefengraber, M., Hendrick, F., Pazmiño, A., Bais, A., Bazureau, A., Boersma, K. F., Bognar, K., Dehn, A., Donner, S., ... Zehner, C. (2021). Ground-based validation of the Copernicus Sentinel-5P TROPOMI NO₂ measurements with the NDACC ZSL-DOAS, MAX-DOAS and Pandonia global networks. *Atmospheric Measurement Techniques*, 14(1), 481–510. <https://doi.org/10.5194/amt-14-481-2021>
- 850 Wagner, T., Warnach, S., Beirle, S., Bobrowski, N., Jost, A., Puķīte, J., & Theys, N. (2023). Investigation of three-dimensional radiative transfer effects for UV–Vis satellite and ground-based observations of volcanic plumes. *Atmospheric Measurement Techniques*, 16(6), 1609–1662. <https://doi.org/10.5194/amt-16-1609-2023>
- 855 Weather Underground. (2023). *Houston, TX Weather History*.
<https://www.wunderground.com/history/daily/us/tx/houston/KHOU>
- Wiedinmyer, C., Akagi, S. K., Yokelson, R. J., Emmons, L. K., Al-Saadi, J. A., Orlando, J. J., & Soja, A. J. (2011). The Fire INventory from NCAR (FINN): A high resolution global model to estimate the emissions from open burning. *Geoscientific Model Development*, 4(3), 625–641. <https://doi.org/10.5194/gmd-4-625-2011>
- 860